STARS

1-1-2008

Lattice contraction during amorphization by mechanical alloying

C. Suryanarayana
University of Central Florida

Satyajeet Sharma
University of Central Florida

Find similar works at: https://stars.library.ucf.edu/facultybib2000

University of Central Florida Libraries http://library.ucf.edu

Recommended Citation

Suryanarayana, C. and Sharma, Satyajeet, "Lattice contraction during amorphization by mechanical alloying" (2008). *Faculty Bibliography 2000s*. 1041.
https://stars.library.ucf.edu/facultybib2000/1041

University of Central Florida

STARS
Showcase of Text, Archives, Research & Scholarship

Lattice contraction during amorphization by mechanical alloying

C. Suryanarayana, and Satyajeet Sharma

View Online

Export Citation

ARTICLES YOU MAY BE INTERESTED IN

Lattice contraction during amorphization by mechanical alloying

C. Suryanarayana[a)] and Satyajeet Sharma[b)]
*Department of Mechanical, Materials and Aerospace Engineering, University of Central Florida,
Orlando, Florida 32816-2450, USA*

Amorphization has been achieved in blended elemental Fe-based multicomponent alloy powders by mechanical alloying. The effect of Nb addition to the $Fe_{42}Ni_{28}Zr_{10-x}Nb_xB_{20}$ alloy in the composition range of $1-6$ at. % Nb has been investigated and it was shown that the glass-forming ability (GFA) of the alloys, defined as the milling time required to produce an amorphous phase, improved with Nb addition. The improvement was not regular; the highest GFA was achieved at an Nb level of 2 at. %. Associated with the amorphization process, lattice contraction was noted. The processes of occurrence of the amorphous phase in this alloy system, maximum GFA in the alloy with 2 at. % Nb, and lattice contraction were explained on the basis of the atomic strain model developed first for binary alloys and extended later to ternary and multicomponent alloys, and the change in coordination number with the size ratio of the constituent atoms. © *2008 American Institute of Physics*. [DOI: 10.1063/1.3020531]

I. INTRODUCTION

Metallic glasses or amorphous alloys are solid materials in which the constituent atoms are arranged in a random manner with no long-range periodicity. Since their first synthesis in a Au–Si eutectic alloy in 1960 by Klement *et al.*[1] metallic glasses were synthesized in a number of binary, ternary, and higher-order alloy systems. These metallic glasses have interesting combination of physical, chemical, mechanical, and magnetic properties, which make them attractive for different applications. As a result, there has been significant interest in understanding the structure and properties of these materials for the last few decades.[2–6] High cooling rates of $>10^5$ K/s were required to produce glassy alloys in the past and consequently the products of rapid solidification processing (RSP) were in the form of flakes, ribbons, or powders with section thicknesses of less than about 50 μm. By increasing the number of components in the alloy system and choosing the appropriate compositions, the critical cooling rate required to produce glassy alloys has been brought down to as low as $10^{-1}-10^2$ K/s (Ref. 7). This, along with the development of new casting techniques, led to the synthesis of glassy alloys with a diameter of several tens of millimeters.[7–11] Such alloys with a large section thickness and high glass-forming ability (GFA) are now referred to as bulk metallic glasses (BMGs). The largest section thickness (or diameter) of a rod that could be produced in a fully glassy condition is 72 mm in a water-quenched Pd-30 at. % Cu-10 at. % Ni-20 at. % P alloy.[12] However, for the successful synthesis of new and improved alloy compositions that could be cast into still thicker sections in a fully glassy state, it is of fundamental importance to understand the reasons for and also to be able to predict or empirically determine alloy compositions that have high GFA. Al-

ternately, a clear knowledge of the mechanism of glass formation would also help in synthesizing better glassy alloys.

Glass formation in an alloy system is complex and therefore it is difficult to correctly predict the GFA of alloys. However, consistent efforts in this direction led to the development of a few simple criteria based upon the most important requirement for glass formation, viz., that formation of a crystalline phase needs to be completely suppressed or avoided on solidification from the melt. Even though a number of criteria have been developed to explain the GFA of liquid alloys, the most important ones were as follows:

(i)   the critical cooling rate for glass formation; the lower the critical cooling rate the higher is the GFA, and

(ii)   the reduced glass transition temperature, T_{rg} ($=T_g/T_l$, where T_g is the glass transition temperature and T_l is the liquidus temperature); the higher the T_{rg} value the higher is the GFA.[13,14]

As a corollary to the second criterion, deep eutectic compositions were found to be most prone to glass formation. Inoue *et al.*[7,15,16] proposed three criteria that need to be satisfied to form the BMGs, viz., (a) a minimum of three components, (b) significant ($>12\%$) difference in atomic sizes of the constituent elements, and (c) large negative heats of mixing among the constituent elements. However, since it was not possible to satisfactorily explain glass formation in different alloy systems, especially the high GFA of some of the BMG alloys, a number of new criteria have been proposed during the last few years.[17–26] The important criteria based on the glass transformation temperatures are summarized in Table I. Among these, although not perfect and some exceptions have been noted, the γ parameter,[18,19] defined as $\gamma = T_{x1}/(T_g+T_l)$, where T_{x1} is the first crystallization temperature of the glassy alloy, seems to most satisfactorily explain the GFA of a majority of the alloys.

Mechanical alloying (MA) is a technique that involves

a)Electronic mail: csuryana@mail.ucf.edu.
b)Present address: Sulzer Metco (US), Inc., Westbury, New York 11590,
 USA.

TABLE I. Summary of the quantitative criteria proposed to evaluate the GFA of liquid alloys.

GFA parameter	Equation	Ref.
T_{rg}	$T_{rg} = T_g / T_l$	13 and 14
ΔT_x	$\Delta T_x = T_x - T_g$	15 and 16
α	$\alpha = T_x / T_l$	17
β	$\beta = 1 + (T_x/T_l) = 1 + \alpha$	17
γ	$\gamma = T_x / (T_g + T_l)$	18 and 19
γ_m	$\gamma_m = (2T_x - T_g) / T_l$	20
δ	$\delta = T_x / (T_l - T_g)$	21
ϕ	$\phi = T_{rg}(\Delta T_x / T_g)^{0.143}$	22
β_m	$\beta_m = (T_x \times T_g) / (T_l - T_x)^2$	23

repeated cold welding, fracturing, and rewelding of powder particles in a high-energy ball mill. It has been shown that this technique is capable of producing all the metastable constitution effects achievable by RSP.[27,28] Additionally, since MA is carried out at room or near-room temperature, the restrictions imposed by phase diagrams are not applicable and therefore it is possible to achieve alloying between metals that are usually immiscible.[27,28] A specific advantage of MA as applied to metallic glassy alloys is that the limitation of section thickness noted in solidification methods can be easily overcome. This is because the amorphous powders produced by MA could be consolidated into bulk shapes of any size in the temperature interval between T_g and T_x, i.e., in the supercooled liquid region, where the viscosity of the alloy is very low. Further, it appears that the mechanism by which an amorphous phase is formed is different between solid-state processed and liquid-state processed alloys.

It was recently reported by Park et al.[29,30] that addition of an alloying element with a positive heat of mixing with a constituent element in a given alloy system improves the GFA and also the plasticity of the inherently brittle glassy alloy. As part of a detailed study on the synthesis and characterization of Fe-based BMGs by the technique of MA, we have recently synthesized a number of glassy alloys by this technique.[26,31–34] Therefore, it was decided to investigate whether the GFA of the Fe-based alloys could also be enhanced by adding an element that has a positive heat of mixing with one of the constituent elements. While successfully increasing the GFA of the alloy by adding Nb,[35] we have also identified that the onset of glass formation is associated with a lattice contraction. Thus, the aim of the present paper is to relate the GFA of the Fe-based Fe–Ni–Zr–Nb–B alloy to the presence of Nb and then discuss the reasons for the formation of an amorphous phase in terms of the lattice strain that occurs during MA. The element Nb was chosen as the alloying element based on its positive heat of mixing with Zr (+17 kJ/mol) and its atomic diameter of 0.2936 nm, which is substantially larger than that of Fe (0.2482 nm) and Ni (0.2492 nm), but smaller than that of Zr (0.3186 nm).

II. EXPERIMENTAL PROCEDURE

Appropriate amounts of the pure elemental metal powders (≥99.9% purity) of Fe, Ni, Zr, Nb, and B were weighed out and mixed together to obtain the desired composition of

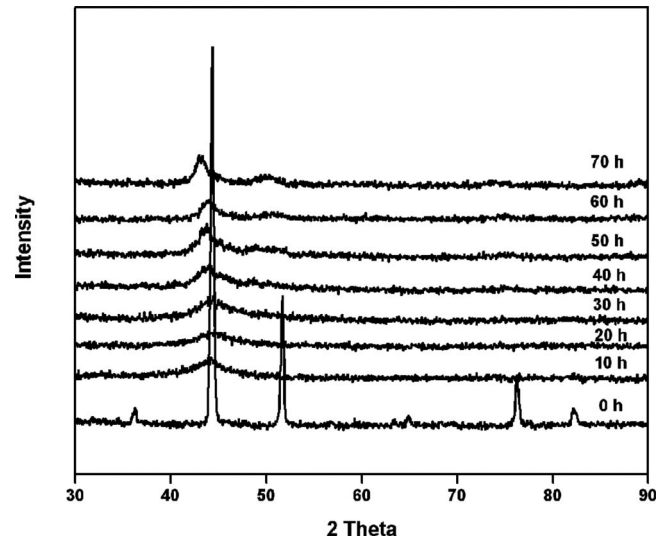FIG. 1. XRD patterns of blended elemental powder mix of $Fe_{42}Ni_{28}Zr_{10}B_{20}$ (Nb-free alloy) as a function of milling time. Note that amorphization has started at around 10 h of milling and complete amorphization is seen to occur after about 20 h of milling. Mechanical crystallization of the amorphous powder has taken place on continued milling of the amorphous powder. This is clear from the presence of a relatively sharp peak at an angle corresponding to about 43°.

$Fe_{42}Ni_{28}Zr_{10-x}Nb_xB_{20}$, with $x = 0$, 1, 2, 4, and 6. The subscripts here represent the composition of the element in the powder mix in atomic percentage. MA was conducted in a high-energy SPEX CertiPrep 8000 D shaker mill. For each experiment, 10 g of the blended elemental powder mix and 100 g of hardened stainless steel balls were loaded into the milling container, thus maintaining a ball-to-powder weight ratio of 10:1 during milling. The ball sizes used were of 2 and 4 mm, to achieve better milling conditions. About 1 wt % of stearic acid was added as a process control agent to prevent severe agglomeration of the powder to the vial walls and/or the grinding medium. The weighing, blending, loading, and unloading of the powders were carried out inside a glovebox with a controlled atmosphere of argon gas, so as to minimize powder contamination.

The phase evolution during milling was monitored by x-ray diffraction (XRD) using a Rigaku x-ray diffractometer with Cu $K\alpha$ radiation ($\lambda = 0.15\,406$ nm) at 40 kV and 35 mA settings. The XRD patterns were recorded in the 2θ range of $30°-90°$. To check the reliability of peak positions, the XRD unit was calibrated with a standard material (pure quartz), and occasionally the reference material was also mixed with the milled powder. The peak positions in the XRD patterns were determined by fitting the peaks to a Gaussian profile. Identification of the phases present and calculation of the lattice parameter were done using standard XRD procedures.[36] The GFA of the alloy was evaluated in terms of the milling time required to form the glassy phase. The GFA was considered higher if amorphization was achieved in a shorter milling time.

III. RESULTS

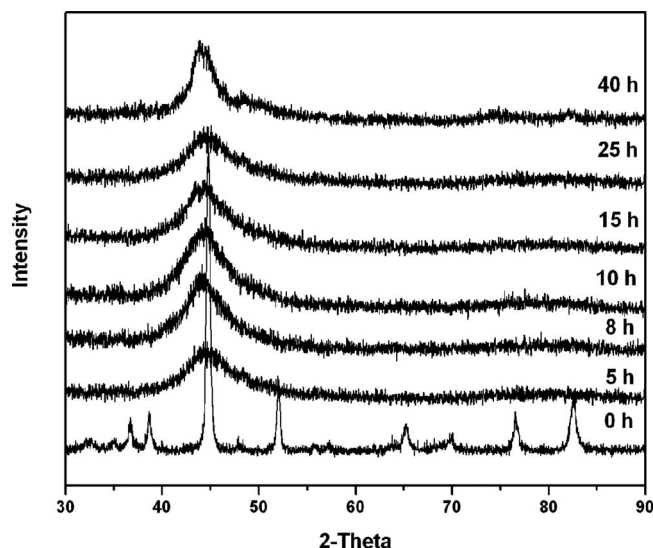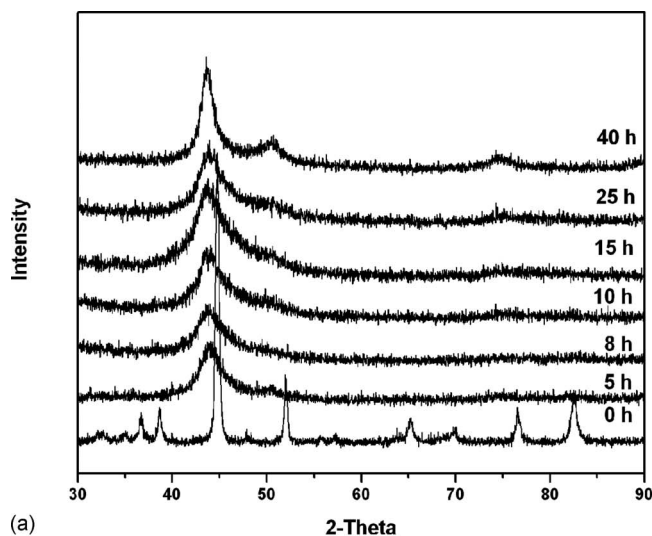Figure 1 shows the XRD patterns of the blended elemental powder mixture of $Fe_{42}Ni_{28}Zr_{10-x}Nb_xB_{20}$, with $x = 0$ (i.e.,

FIG. 2. XRD patterns of blended elemental powder mix of $Fe_{42}Ni_{28}Zr_8Nb_2B_{20}$ as a function of milling time. Note the formation of an amorphous phase on milling the powders for 5 h. Also note the shift in the broad peak position on milling the powder for 8 and 10 h.

Nb-free alloy), as a function of milling time. While all the expected diffraction peaks of Fe, Ni, and Zr are seen in the as-blended powder i.e., without any milling), boron peaks are not seen because of its low scattering factor and also because it is amorphous. On the other hand, the powder blend milled for 20 h clearly shows that complete amorphization of the powder mix has occurred, as evidenced by the presence of a broad diffuse peak at the angular position corresponding to the position of the crystalline $(110)_{Fe}$ peak. Transmission electron microscopy and diffraction studies have confirmed the presence of an amorphous phase in the powder milled for 20 h. However, on further milling, devitrification of the amorphous phase is seen to start after about 40 h of milling, as indicated by sharpening of the diffuse peak and occurrence of new low intensity peaks. This phenomenon, referred to as mechanical crystallization,[32] has also been noted in other powder blends subjected to MA.[31,33] The time gap between the formation of the amorphous phase and its crystallization on continued milling can be considered as a measure of the stability of the amorphous phase during MA.

Figure 2 shows the XRD patterns of the $Fe_{42}Ni_{28}Zr_{10-x}Nb_xB_{20}$ powder mix, with $x=2$, as a function of milling time. It is noted that complete amorphization has taken place on milling the powder for 5–8 h and that the amorphous phase is stable till 10 h of milling time. Thus, it may be noted that the GFA of the powder mix has improved with increasing Nb content, noting, however, that the stability of the amorphous phase is lower in this alloy in comparison to that in the Nb-free alloy.

An important observation made during the experiment is that the position of the diffuse peak, representing the amorphous phase that has formed on MA, has changed as a function of milling time. To get a better appreciation of the peak shifts, the x-ray broad peaks were fitted to a Gaussian profile and the 2θ values of the peak were determined.

Figure 3 shows the XRD patterns of the

(a)
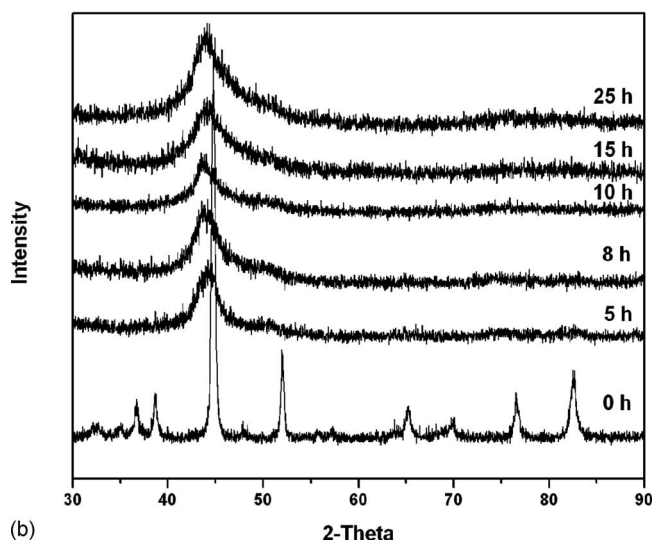
(b)

FIG. 3. XRD patterns of the blended elemental powder mix of $Fe_{42}Ni_{28}Zr_{10-x}Nb_xB_{20}$ as a function of milling time. Note that formation of the amorphous phase now occurs at 10 h in the powder blend with $x=4$ (a) and at 15 h for the powder blend with $x=6$ (b). That is amorphous phase formation is significantly delayed in the powder blend with $x=6$. Further, similar to the other compositions, the broad peak indicating formation of the amorphous phase has shifted with milling time.

$Fe_{42}Ni_{28}Zr_{10-x}Nb_xB_{20}$ powder mix, with $x=4$ [Fig. 3(a)] and $x=6$ [Fig. 3(b)], as a function of milling time. Note that the times required for the formation of the amorphous phase in these powder blends are different. While the amorphous phase had formed in about 10 h in the blend with $x=4$, it had formed at a longer time of milling, viz., 15 h in the blend with $x=6$. This time is much longer than in the other powder blends containing Nb, and is in fact the longest. Thus, it can be concluded that even though Nb addition has helped in increasing the GFA, the magnitude of improvement was different at different Nb levels. Thus, while the time required for the formation of the amorphous phase in the $Fe_{42}Ni_{28}Zr_{10-x}Nb_xB_{20}$ powder mix, with $x=0$ (i.e., Nb-free alloy) was 20 h, it decreased to 10 h for $x=1$, 8 h when $x=2$, 10 h for $x=4$, and 15 h for $x=6$. Stated differently, the maximum GFA was achieved when $x=2$ (Fig. 4).

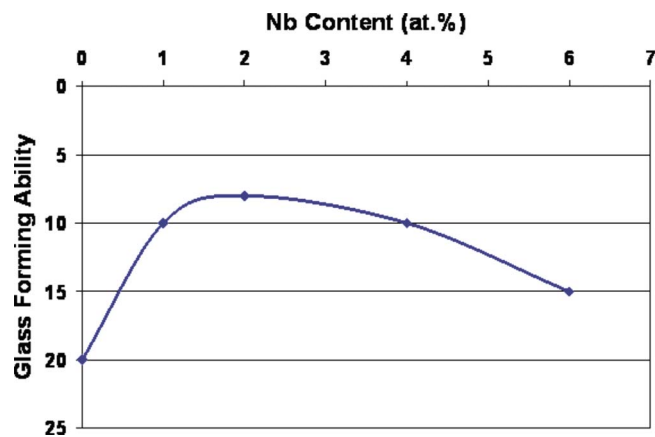Again, similar to the powder blend containing 2 at. %

FIG. 4. (Color online) GFA as a function of Nb content in the $Fe_{42}Ni_{28}Zr_{10-x}Nb_xB_{20}$ powder blends. The GFA was evaluated as the time required for amorphous phase formation. The shorter the time required the higher is the GFA.

FIG. 5. (Color online) Variation of the 2-θ values corresponding to the diffuse broad peak with milling time for the different $Fe_{42}Ni_{28}Zr_{10-x}Nb_xB_{20}$ powder blends with $x=1$, 2, 4, and 6 at. %. The arrow corresponds to the time when the amorphous phase formation has been observed.

Nb, the position of the diffuse peak representing the amorphous phase has shifted with milling time. The values of 2θ as a function of milling time are listed in Table II for different compositions. It is clear from this table that the variation of the peak position with milling time is different, and that it is also dependent on the Nb content in the powder blend. The variation of the 2θ value with milling time for the powder blends with different Nb contents is shown in Fig. 5.

It is clear from Fig. 5 that during the early period of milling, the 2θ value corresponding to the broad diffuse peak decreases with milling time. This is an expected trend since dissolution of atoms with larger atomic diameters (e.g., Ni, Zr, and Nb) in the Fe solid solution dilates the lattice, increases the lattice parameter and therefore, the peaks shift to lower angular positions in the XRD patterns. On continued milling, the 2θ value had unexpectedly shifted to higher angular positions and this coincided with the amorphization of the powder. The arrow marks in the figure show the milling times at which the amorphous phase formation was observed. This observation is quite fascinating since it indicates the occurrence of lattice contraction during amorphization.

IV. DISCUSSION

The XRD patterns presented in Figs. 1–3 and the results mentioned above clearly show that addition of Nb has a significant effect on the GFA of $Fe_{42}Ni_{28}Zr_{10-x}Nb_xB_{20}$ powder mixtures on milling. The results show that addition of Nb has increased the GFA of mechanically alloyed Fe-based alloys. However, the improvement is not uniform; the amount of Nb
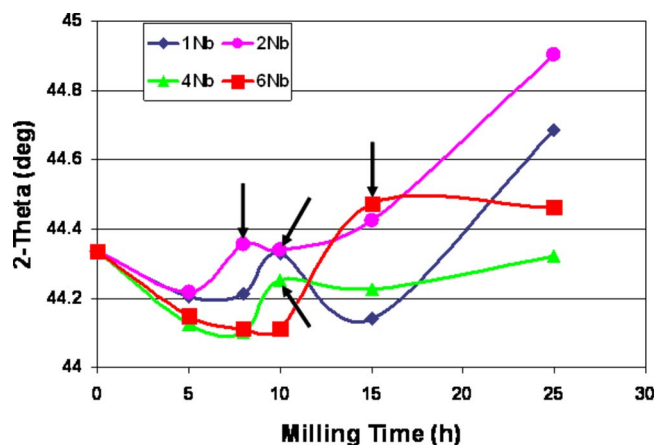
added appears to determine the GFA. The GFA improved with increasing addition of Nb and then decreased on increasing the Nb beyond about 2 at. %. Therefore, it becomes important for us to know the reasons for

- the increase in GFA due to Nb addition, and
- the maximum in the GFA in alloys containing 2 at. % Nb.

Additionally, and more interestingly, we should also rationalize the lattice contraction that is associated with amorphization in these powder blends.

A. Role of Nb in increasing GFA

While discussing the role of Nb in increasing the GFA of Fe-based powder blends, it may be useful to discuss it under two different conditions—first, its role as an element that has an atomic size different from the other elements in the powder mix and second, as an element that has a positive heat of mixing with Zr. This will determine which of these two factors is more important in increasing the GFA.

It has been well known in literature on metallic glasses that atomic sizes of the constituent atoms in the alloy play a critical role on glass formation. As mentioned earlier, one of the Inoue criteria is that the constituent elements should differ in their atomic sizes by >12%. Significant differences in the sizes of elements constituting the amorphous alloy has been known to be important in formation of metallic glasses.[2–5] Cahn[5] referred to this as the anti-Hume–Rothery

TABLE II. 2θ values corresponding to the broad diffuse peak representing the amorphous phase in the $Fe_{42}Ni_{28}Zr_{10-x}Nb_xB_{20}$ powder blends as a function of milling time.

Nb Content, x (at. %)	2θ values of the broad peak at different milling times					
	0 h	5 h	8 h	10 h	15 h	25 h
$x=1$	44.79	44.21	44.21	44.33	44.14	44.69
$x=2$	44.79	44.22	44.36	44.34	44.43	44.90
$x=4$	44.79	44.13	44.10	44.25	44.23	44.32
$x=6$	44.79	44.15	44.11	44.11	44.47	44.46

rule since the Hume–Rothery rules predict that extensive solid solutions form in binary alloy systems, especially those based on noble metals, when the constituent atoms differ in their atomic sizes by <15%.

The presence of different sizes of atoms in an alloy helps in efficient packing of atoms and increase the viscosity of the melt and both these effects have been found to be beneficial in the formation of metallic glasses.[7,24,37–40] However, since a liquid phase is not involved during amorphization by MA (which is a completely solid-state processing method), this argument will not be useful in explaining the increased GFA of the present Fe-based alloy by Nb addition. But, it should be noted that the presence of atoms of different sizes introduces significant strain into the crystal lattice and it is this increase in the strain energy that raises the free energy of the crystalline phase (above that of the hypothetical amorphous phase), which helps in the stabilization of the amorphous phase. We will discuss this further in the later sections.

Preliminary investigations suggest that the positive heat of mixing between Nb and Zr does not appear to directly help in increasing the GFA of the alloy, even though there are examples in the literature where alloys containing immiscible elements (elements that have a positive heat of mixing between them) can be made amorphous by MA.[41] However, more investigations need to be carried out to validate this conclusion further. Thus, it appears that the increased GFA of the Fe-based alloys in the present investigation is more probably related to the large difference in the atomic sizes of the constituent elements than the positive heat of mixing. Let us now try to understand the reasons for (i) amorphization in this system, (ii) the effect of Nb addition on the increased GFA, and (iii) the associated lattice contraction behavior.

B. Reasons for amorphization

It has been frequently mentioned in literature that amorphization by MA is possible when the free energy of the crystalline phase can be increased to a level above that of the hypothetical amorphous phase.[27,28] The increase in free energy of the crystalline phase can be achieved through incorporation of lattice defects such as vacancies, dislocations, grain boundaries, etc., or disordering of intermetallics, and/or the lattice strain introduced into the system. While only a qualitative or an approximate estimate of the contribution of the crystalline defects to the increase in the free energy of the crystal lattice can be made, it is possible to determine, at least semiquantitatively, the contribution of lattice strain, using the models of Egami and subsequently developed further by others.

Egami and Waseda[42] proposed a model to calculate the lattice strain obtained in a binary alloy by the introduction of a solute atom of a size different from that of the solvent atom. Using the atomic scale elasticity theory, they calculated the atomic level stresses in both the solid solution and an amorphous phase. They noted that neither the local stress fluctuations nor the total strain energy varied much with solute concentration in the amorphous alloy. On the other hand, the strain energy increased continuously and linearly with solute content in the solid solution. Thus, beyond a critical

solute concentration, the glassy alloy becomes energetically more favorable than the corresponding crystalline lattice. This minimum solute concentration necessary to obtain the stable glassy phase, $C_B^{\min}$, was found to be inversely correlated with the atomic volume mismatch, $(v_B - v_A)/v_A$, where v_A is the atomic volume of the matrix atom A and v_B is the atomic volume of the solute atom B, according to the relationship

$$\left| \frac{(v_B - v_A)}{v_A} \right| C_B^{\min} = 0.1. \tag{1}$$

From the above analysis, it becomes clear that the presence of solute atoms is necessary to form an amorphous phase. In fact, Egami[43] emphasized that "*In general, alloying makes glass formation easier, not because alloying stabilizes a glass, but because it destabilizes a crystal.*"

This concept of a critical strain required to destabilize a crystalline lattice, originally developed for binary alloys was later extended to the case of ternary alloy systems[44] and multicomponent BMGs.[45] This model was further developed by Miracle *et al.*[46,47] who brought in the concept of local clustering of solvent atoms around the solute atom in order to achieve dense random packing. They also proposed that a crystalline lattice becomes unstable once the internal strain reaches a critical value causing a change in the local coordination number.[37] Another important difference between the models of Egami and Miracle is that while the Egami model assumed that all the solute elements, irrespective of their size, take up the substitutional positions, the model of Miracle accounts for the occupancy of either substitutional or interstitial positions depending on the size of the solute atom.

In the present case, the volumetric strain in the Fe solid solution lattice due to solute addition was calculated using the equations

$$\varepsilon_V^A = \frac{2}{3}\left(\frac{1-2\nu}{1-\nu}\right)\lambda_1, \tag{2}$$

where ε_V^A is the volumetric strain, λ_1 is the mismatch between solute atoms and coordination hole of the nearest neighbor atoms in the multicomponent system, ν is Poisson's ratio, and

$$\lambda_1 = \frac{\sum y_i C_i}{1 + \sum C_i(y-1)}\left[\left(\frac{2}{\sum (1+R)}\right)^3 - 1\right], \tag{3}$$

where y is the ratio of deformed volume of solute and solvent as given below, $R = R_{\text{solute}}/R_{\text{solvent}}$ and C_i is the atomic concentration of the ith element, and y is given by

$$y = R^3\left[\frac{2}{3}\left(\frac{1-2\nu}{1-\nu}\right)\left(\frac{2}{1+R}\right)^3 + \frac{1+\nu}{3(1-\nu)}\right]. \tag{4}$$

Values of ε_V^A calculated using the above equations for the different Nb contents with $x=1$, 2, 4, and 6 at. % are shown in Table III.

It is clear from Table III that the absolute value of the volumetric strain is greater than 0.054, the critical value above which it leads to topological instability of the lattice in

TABLE III. Volumetric strain for the $Fe_{42}Ni_{28}Zr_{10-x}Nb_xB_{20}$ system with x =1, 2, 4, and 6 at. %, calculated using Eqs. (2)–(4).

at. % Nb	Volumetric strain
1	−0.191 83
2	−0.191 14
4	−0.189 74
6	−0.188 31

the crystalline matrix, sufficient enough to cause amorphization. This explains why amorphization has been achieved in all the powder mixes by MA.

From the above analysis it becomes clear that by introduction of solute atoms of different size into the Fe lattice, it was possible to develop sufficient amount of strain in the lattice to make it amorphous. However, the process of MA is also known to additionally introduce crystal defects which also raise the energy of the system. Thus, the reason for the occurrence of amorphization in this alloy system could be due to both the above effects. Hence, in all likelihood, it is the size difference between the constituent atoms in the system which is more important in allowing this system to go into the amorphous state. This is because the contribution of lattice defects to raise the energy of the system is rather low.[26] The negative values of the volumetric strain support the fact that amorphization is accompanied by a contraction of the lattice, which has been demonstrated experimentally.

C. Highest GFA at 2 at. % Nb

The diffraction angle for the broad diffuse peak from the amorphous phase is related to the interatomic distance, X_m through the Bragg relation

$$1.23\lambda = 2X_m \sin \theta, \tag{5}$$

where λ is the wavelength of the x-ray beam used, X_m is the interatomic distance between the neighboring atoms, θ is the peak position, and 1.23 is the correction factor used for liquids and amorphous solids.[48] Using this relation, the distance between nearest neighbor atoms has been calculated and these values are listed in Table IV for the amorphous alloys with different Nb contents. Since the scattering intensity of the metalloid atom (boron, in the present case) is significantly lower in comparison to that of the transition metal (TM) atoms, X_m obtained from the above equation can be considered as the average TM-TM nearest neighbor atomic distance. It is clear from Table IV that addition of Nb results

TABLE IV. Interatomic distances between TM atoms in the $Fe_{42}Ni_{28}Zr_{10-x}Nb_xB_{20}$ system; 2θ corresponds to the position of the broad diffuse peak at the time of amorphization and X_m is the average interatomic distance between TM atoms.

at. % Nb	Time for amorphization (h)	2θ (deg)	X_m (nm)
1	10	44.33	0.2511
2	8	44.36	0.2517
4	10	44.25	0.2515
6	15	44.47	0.2503

TABLE V. R and N values for individual solute atoms in the amorphous $Fe_{42}Ni_{28}Zr_{10-x}Nb_xB_{20}$ system. ($R=R_B/R_A$, where R_A is the radius of solvent atom, R_B is the radius of solute atom, and N is the coordination number of the first shell).

Element	Radius (nm)	$R=R_B/R_{Fe}$	Occupancy	N
Fe	0.1241			
Ni	0.1246	1.004	Substitutional	13
Zr	0.1593	1.284	Substitutional	18
Nb	0.1468	1.183	Substitutional	16
B	0.0820	0.661	Interstitial	9

in increased TM-TM nearest neighbor atom distance, i.e., an increase in topological instability, and that the TM-TM distance is larger for the alloys with 2 and 4 at. % Nb, and is the highest for the amorphous alloy with 2 at. % Nb. Further, it is seen from the diffraction patterns that the *width* of the diffuse peak, representing the amorphous phase, is maximum in the powder blend containing 2 at. % Nb. This observation lends further support to the increased GFA of the alloy at this composition (with 2 at. % Nb) through further enhancement of topological disorder in the alloy system. Thus, the increased nearest neighbor distance and the larger width of the broad diffuse peak satisfactorily explain the highest GFA observed in the $Fe_{42}Ni_{28}Zr_8Nb_2B_{20}$ powder blend, as evidenced by the shortest time (5–8 h) required for amorphization among all the alloy compositions investigated.

D. Reasons for lattice contraction

Our study involves Fe as the matrix (solvent atom) with Ni, Zr, Nb, and B being the solute atoms. According to Miracle's model, the solute atoms, at room temperature, get distributed between the substitutional and interstitial sites depending on the radius ratio $R=R_B/R_A$, where A represents the solvent atom and B is the solute atom. The model suggests that when $R<0.8$, the solute atoms occupy the interstitial sites and when $R>0.83$, they occupy the substitutional sites. At intermediate values of R, the solute atoms occupy either the interstitial or substitutional sites. Further, this model showed a strong correlation between R and N, the coordination number of the first nearest neighbor shell.[47] Table V shows the R and N values corresponding to the individual solute atoms in the given Fe-based multicomponent system. Even though the coordination numbers are more accurately related to the R^* values, the corresponding R values with maximum packing efficiency, with the accuracy of first decimal place it is possible to estimate the N value for individual solute atoms with the corresponding R value.

Based on the data from Table V we can explain the occurrence of lattice contraction during amorphization. In the $Fe_{42}Ni_{28}Zr_{10-x}Nb_xB_{20}$ system the possible values of N for the different solute atoms (atomic clusters—solvent atoms surrounding solute atom) during amorphization are calculated to be 13, 18, 16, and 9 for Ni, Zr, Nb, and B, respectively. When Zr is replaced by Nb the coordination number changes from 18 to 16 leading to a matrix with more efficient

packing and less free volume. This occurrence leads to contraction of the lattice during amorphization and is supported by the shift of 2θ values of the broad diffuse peak to higher angles with an increase in milling time. However, at very high Nb content, e.g., at 6 at. % Nb, the GFA of the alloy decreases (as evidenced by the longer time required for amorphization) associated with a decrease in the TM-TM distance. In other words, topological instability is less favorable toward amorphization.

Amorphization has been reported in a number of materials—both metallic and nonmetallic.[49] One of the ways in which amorphization has been achieved is through the application of high pressures, more popular for nonmetallic materials.[50] For example, it has been reported that zirconium tungstate (ZrW_2O_8) could be amorphized by subjecting the compound to a high pressure in the range of 1.5–3.5 GPa.[51] Since this compound is a framework structure and also exhibits a negative thermal expansion, it was suggested that there could be a relationship between the negative thermal expansion and pressure-induced amorphization in such compounds. In fact, computer simulations pointed out the possibility of a common origin between pressure-induced amorphization and negative thermal expansion in tetrahedrally bonded networks,[52] Therefore, it is possible that "lattice" contraction (resulting in smaller volumes) is associated with the process of amorphous phase formation. It has been reported that the pressures developed during MA experiments can be as high as 6 GPa (Ref. [28]), and therefore it is possible that these high pressures could also contribute to reduced volumes and hence the process of amorphization. Although, the relationship between negative thermal expansion and pressure-induced amorphization has been established for network-type structures, and extending this to metallic-type alloys could be risky, it may be argued that metallic glassy alloys also have been shown to be consisting of clusters in the liquid state[37] and that these clusters could be considered as structural units.

V. CONCLUSIONS

Blended elemental powder mixtures corresponding to the compositions of $Fe_{42}Ni_{28}Zr_{10-x}Nb_xB_{20}$ with $x=0$, 1, 2, 4, and 6 at. % have been shown to become amorphous on milling them in a high-energy ball mill. It has been shown that addition of Nb improves the GFA of the alloys. The highest GFA (in terms of the milling time required for amorphization) was noted for the $Fe_{42}Ni_{28}Zr_8Nb_2B_{20}$ alloy. Associated with the amorphization, the 2θ value of the broad diffuse peak representing the amorphous phase in the XRD pattern showed a maximum value representing lattice contraction. The reasons for amorphization, improvement of the GFA on Nb addition, and the possible causes for lattice contraction have been discussed using the concept of local topological instability as proposed by Egami and further developed by Miracle. It is suggested that lattice contraction could be related to the phenomenon of pressure-induced amorphization in framework structures that exhibit the phenomenon of negative thermal expansion.

[1] W. Klement, Jr., R. H. Willens, and P. Duwez, Nature (London) **187**, 869 (1960).
[2] *Amorphous Metallic Alloys*, edited by F. E. Luborsky (Butterworths, London, 1983).
[3] *Metallic Glasses: Production, Properties and Applications*, edited by T. R. Anantharaman (Trans Tech, Zurich, 1984).
[4] C. Suryanarayana, Bull. Mater. Sci. **6**, 579 (1984).
[5] R. W. Cahn, in *Materials Science and Technology: A Comprehensive Treatment*, edited by J. Zarzycki (VCH, Weinheim, 1991), Vol. 9, pp. 493–548.
[6] *Rapidly Solidified Alloys: Processes, Structures, Properties, Applications*, edited by H. H. Liebermann (Marcel Dekker, New York, 1993).
[7] A. Inoue, Acta Mater. **48**, 279 (2000).
[8] W.L. Johnson, MRS Bull. **24**, 42 (1999).
[9] J. F. Löffler, Intermetallics **11**, 529 (2003).
[10] A. Inoue, *Bulk Amorphous Alloys: Preparation and Fundamental Characteristics*, Materials Science Foundations Vol. 4 (TransTech, Zurich, 1998).
[11] A. Inoue, *Bulk Amorphous Alloys: Practical Characteristics and Applications*, Materials Science Foundations Vol. 6 (TransTech, Zurich, 1999).
[12] A. Inoue, N. Nishiyama, and H. M. Kimura, Mater. Trans., JIM **38**, 179 (1997).
[13] M. H. Cohen and D. Turnbull, Nature (London) **189**, 131 (1961).
[14] D. Turnbull, Contemp. Phys. **10**, 473 (1969).
[15] A. Inoue, T. Zhang, and T. Masumoto, J. Non-Cryst. Solids **156–158**, 473 (1993).
[16] A. Inoue, Mater. Trans., JIM **36**, 866 (1995).
[17] K. Mondal and B. S. Murty, J. Non-Cryst. Solids **351**, 1366 (2005).
[18] Z. P. Lu and C. T. Liu, Acta Mater. **50**, 3501 (2002).
[19] Z. P. Lu and C. T. Liu, Phys. Rev. Lett. **91**, 115505 (2003).
[20] X. H. Du, J. C. Huang, C. T. Liu, and Z. P. Lu, J. Appl. Phys. **101**, 086108 (2007).
[21] Q. J. Chen, J. Shen, D. Zhang, H. B. Fan, J. F. Sun, and D. G. McCartney, Mater. Sci. Eng., A **433**, 155 (2006).
[22] G. J. Fan, H. Choo, and P. K. Liaw, J. Non-Cryst. Solids **353**, 102 (2007).
[23] Z. Z. Yuan, S. L. Bao, Y. Lu, D. P. Zhang, and L. Yao, J. Alloys Compd. **459**, 251 (2008).
[24] D. B. Miracle, Nature Mater. **3**, 697 (2004).
[25] S. Azad, A. Mandal, and R. K. Mandal, Mater. Sci. Eng., A **458**, 348 (2007).
[26] S. Sharma, R. Vaidyanathan, and C. Suryanarayana, Appl. Phys. Lett. **90**, 111915 (2007).
[27] C. Suryanarayana, Prog. Mater. Sci. **46**, 1 (2001).
[28] C. Suryanarayana, *Mechanical Alloying and Milling* (Marcel Dekker, New York, 2004).
[29] E. S. Park, D. H. Kim, T. Ohkubo, and K. Hono, J. Non-Cryst. Solids **351**, 1232 (2005).
[30] E. S. Park and D. H. Kim, Acta Mater. **54**, 2597 (2006).
[31] U. Patil, S. J. Hong, and C. Suryanarayana, J. Alloys Compd. **389**, 121 (2005).
[32] S. Sharma and C. Suryanarayana, J. Appl. Phys. **102**, 083544 (2007).
[33] S. Sharma and C. Suryanarayana, J. Appl. Phys. **103**, 013504 (2008).
[34] S. Sharma and C. Suryanarayana, Scr. Mater. **58**, 508 (2008).
[35] S. Sharma, Ph.D. Dissertation, University of Central Florida, 2008.
[36] C. Suryanarayana and M. G. Norton, *X-Ray Diffraction: A Practical Approach* (Plenum, New York, 1998).
[37] D. B. Miracle, Acta Mater. **54**, 4317 (2006).
[38] D. B. Miracle, W. S. Sanders, and O. N. Senkov, Philos. Mag. **83**, 2409 (2003).
[39] P. K. Gupta and D. B. Miracle, Acta Mater. **55**, 4507 (2007).
[40] A. N. Alcaraz, R. S. Duhau, J. R. Fernández, P. Harrowell, and D. B. Miracle, J. Non-Cryst. Solids **354**, 3171 (2008).
[41] E. Ma, Prog. Mater. Sci. **50**, 413 (2005).
[42] T. Egami and Y. Waseda, J. Non-Cryst. Solids **64**, 113 (1984).
[43] T. Egami, J. Non-Cryst. Solids **205–207**, 575 (1996).
[44] Z. J. Yan, J. F. Li, S. R. He, and Y. H. Zhou, Mater. Res. Bull. **38**, 681 (2003).

[45]T. Egami, J. Non-Cryst. Solids **317**, 30 (2003).
[46]D. B. Miracle and O. N. Senkov, Mater. Sci. Eng., A **347**, 50 (2003).
[47]D. B. Miracle, O. N. Senkov, W. S. Sanders, and K. L. Kendig, Mater. Sci. Eng., A **375–377**, 150 (2004).
[48]A. Guinier, *X-ray Diffraction in Crystals, Imperfect Crystals and Amorphous Bodies* (W. H. Freeman, San Francisco, CA, 1963), pp. 72–81.
[49]*Glasses and Amorphous Materials*, Materials Science and Technology: A Comprehensive Treatment Vol. 9, edited by J. Zarzycki (VCH, Weinheim, 1991).
[50]S. M. Sharma and S. K. Sikka, Prog. Mater. Sci. **40**, 1 (1996).
[51]C. A. Perottoni and J. A. H. da Jornada, Science **280**, 886 (1998).
[52]R. J. Speedy, J. Phys.: Condens. Matter **8**, 10907 (1996).